Eur. Phys. J. B **13**, 245–256 (2000)

THE EUROPEAN PHYSICAL JOURNAL B

EDP Sciences

Study of the positive muon Knight shift in UNi_2Al_3: Evidence for a tetravalent U^{4+}-state and crystalline electric field splitting

A. Schenck[1,a], N.K. Sato[2], G. Solt[3], D. Andreica[1], F.N. Gygax[1], M. Pinkpank[1], and A. Amato[3]

[1] Institute for Particle Physics of ETHZ, 5232 Villigen PSI, Switzerland
[2] Physics Department, Graduate School of Science, Tohoku University, Sendai 980-8578, Japan
[3] Paul Scherrer Institute (PSI), 5232 Villigen PSI, Switzerland

Received 20 April 1999

Abstract. We report on transverse field (TF) Muon Spin Rotation (μSR) measurements on a single crystal of the hexagonal heavy fermion superconductor UNi_2Al_3 between 5 K and 300 K. From the measured muon (μ^+) Knight shift (KS) in the easy (a,b)-plane and along the c-axis we extracted the local magnetic susceptibility tensor $\overleftrightarrow{\chi}_{\rm local}$, which arises from the nearest U-neighbors. By comparison with the bulk susceptibility $\overleftrightarrow{\chi}_{\rm tot}$ it is found that $\overleftrightarrow{\chi}_{\rm loc}$ and $\overleftrightarrow{\chi}_{\rm tot}$ agree well above 150 K but deviate considerably in the basal plane below 150 K, due to the disturbance introduced by the μ^+. We succeed in reproducing both $\overleftrightarrow{\chi}_{\rm tot}\,(T)$ and $\overleftrightarrow{\chi}_{\rm loc}\,(T)$ on the basis of a crystalline electric field (CEF)-approach assuming U to be in the tetravalent (U^{4+}) state. The disturbance introduced by the μ^+ affects the CEF-Hamiltonian in an expected manner, suggesting strongly that a CEF-picture implying a rather local $5f$-electron wave function is indeed valid. Reanalyzing older data on UPd_2Al_3 we arrive at the same conclusion. A necessary condition for extracting the local susceptibility was the knowledge of the μ^+-site, this information was derived from the analysis of the TF-relaxation rates. At low temperatures we found about 30% of the implanted μ^+ at the d-site and none at this site above 200 K. The majority fraction was found to be in a tunneling state over six m (or k)-sites around the b-site. No long range diffusion was seen up to room temperature.

PACS. 76.60.Cq Chemical and Knight shifts – 71.70.Ch Crystal and ligand fields – 76.75.+i Muon spin rotation and relaxation

1 Introduction

The apparent coexistence of superconductivity and magnetic order in certain so called heavy fermion systems, intermetallic compounds based on rare earth (Ce, Yb) or actinide (U) ions, is a rare phenomenon which is still not understood in many respects. It is not even clear whether the Ce- or U-compounds are governed by the same physics. In particular, the meaning of coexistence is ambiguous: is it of a microscopic or a macroscopic nature? Are the same or different electron states involved, associated with heavy or light masses, with different parts of the Fermi surface, with local or itinerant behavior? The hexagonal and isostructural compounds UPd_2Al_3 and UNi_2Al_3 in which the coexistence of magnetic order and superconductivity was discovered eight years ago [1,2] are still of much interest in this respect since, despite their close similarity, both the superconductivity and the magnetic order are quite different and also the paramagnetic phase displays different properties. UPd_2Al_3 orders below $T_{\rm N} = 14.5$ in a simple antiferromagnetic structure, consisting of ferromagnetically arranged moments in the (a,b)-planes which are stacked antiferromagnetically [3]. The ordered moment amounts to $\sim 0.85\ \mu_{\rm B}$. The compound becomes superconducting below $T_{\rm c} \simeq 2$ K and, as shown by neutron scattering, the magnetic and superconducting order parameters are not independent of each other [4,5]. In contrast, UNi_2Al_3 develops an incommensurate spin density wave with propagation vector $(\frac{1}{2}\pm\tau, 0, \frac{1}{2})$ ($\tau = 0.11\pm0.003$) and a maximum amplitude of $0.21(1)\mu_{\rm B}$ below $T_{\rm N} = 4.6$ K. Superconductivity sets in at $\sim$ 1.2 K. Again the magnetic and superconducting states are coupled [6,7]. NMR investigations of the spin dynamics in both compounds have revealed pronounced differences [8]. In UNi_2Al_3 the spin lattice relaxation peaks sharply at $T_{\rm N}$, while such a peak, signaling a critical slowing down of the spin dynamics, is absent in UPd_2Al_3. Interestingly, NQR measurements show also no peak in UNi_2Al_3 [9]. In UNi_2Al_3, far above and below $T_{\rm N}$, $1/T_1$ shows the characteristics of a weak itinerant antiferromagnetic system with wave number dependent spin fluctuations, persisting below $T_{\rm N}$ and peaking around the antiferromagnetic wave vector Q [8]. In contrast, in UPd_2Al_3, $1/T_1$ becomes temperature independent above 60 K (a common property in heavy

[a] e-mail: Alexander.Schenck@psi.ch

electron systems) and reflects Fermi liquid behavior (T_1T = const.) far below T_N, *i.e.*, below 4.2 K. In addition, the opening of an energy gap below T_N is indicated [8]. The temperature dependence of $1/T_1$ of both compounds below T_c can well be explained in terms of an anisotropic energy gap model, implying d-wave pairing [8,9].

Several experimental results have provided evidence that in UPd_2Al_3 itinerant (bandlike) as well as local $5f$-electron states coexist [10–12]. The itinerant, "heavy" electrons are thought to be responsible for the superconductivity, while the more local states develop the antiferromagnet order. Corresponding investigations on UNi_2Al_3 are lacking. This dual character of the $5f$-states seems not to be inconsistent with recent band structure calculations using the local spin density functional approximation [13]. This calculations succeed, in particular, in reproducing de Haas van Alphen results [14], and would strongly support an itinerant-electron picture for UPd_2Al_3, but fail to explain quantitatively the very anisotropic magnetic susceptibility χ and its temperature dependence [15].

The magnetic susceptibility χ in UNi_2Al_3 [16] and UPd_2Al_3 [15] are both similar and quite distinct (see also Figs. 10, 11 below). When the external field **B** is applied along the crystalline c-axis, the magnetic susceptibility of both compounds is small and only weakly temperature dependent. In UPd_2Al_3 for **B** applied in the basal (a,b) plane a pronounced maximum in $\chi_\perp$ is observed at ~ 39 K. Above 100 K $\chi_\perp$ follows a Curie-Weiss behavior. In UNi_2Al_3 for the same orientation $\chi_\perp$ is much smaller (at 35 K by a factor of ~ 3) and the now shallow maximum has moved to ~ 110 K. Up to room temperature no Curie-Weiss behavior is observable. The overall behavior of $\overleftrightarrow{\chi}$ in UPd_2Al_3 is very similar to what is observed in the isostructural compound $PrNi_5$ [17]. Here the behavior of $\overleftrightarrow{\chi}$ is fully explained on the basis of the crystal electric field (CEF) splitting of the $4f^2$ $^3H_4$ ground state multiplet of Pr^{3+}, the existence of which is seen also directly in inelastic neutron scattering [18]. This close similarity lead the authors of reference [15] to consider a CEF-picture also for UPd_2Al_3, which implies the presence of a rather local $5f$-electron wave function. Assuming the tetravalent state U^{4+} with $2f$-electrons, like in Pr^{3+}, the measured $\overleftrightarrow{\chi}$ could be very well reproduced, in particular the maximum in $\chi_\perp$ at 38 K. The same CEF-approach provided also a reasonable account for the temperature dependence of the specific heat [19]. A CEF-picture is also not inconsistent with magnetization density measurements with polarized neutrons [20], and recent X-ray magnetic circular dichroism work on UPd_2Al_3 points to strong crystal fields acting on the U-ions [21]. A direct observation of a CEF-split ground state of UPd_2Al_3 may have been seen by inelastic neutron scattering [22], but the evidence appears to be weak, although the excitation energies are consistent with the analysis of reference [15]. Theoretical approaches [13,23] start from an itinerant picture. The situation in UNi_2Al_3 is even less clear, but also in this compound a CEF-scheme was adopted to explain $\overleftrightarrow{\chi}$ [24].

Hence it is deemed important to collect further information which could help in our understanding of the complex behavior of UNi_2Al_3 and UPd_2Al_3. In this paper we report on a μSR-study of monocrystalline UNi_2Al_3 intended to shed light on the question of the importance of CEF-effects or the presence of local $5f$-wave functions versus an itinerant picture. The idea is to measure the modification in the local magnetic response brought about by the presence of the implanted positive muons (μ^+), which act as a local disturbance. The response to this disturbance should depend on the local intrinsic electronic properties. The local magnetic response is monitored *via* the μ^+ Knight shift by measuring with high precision the Larmor frequency in a field applied transversely to the spin polarization of the implanted μ^+ [25]. Similar work has been performed before in $PrNi_5$ [26] and $PrIn_3$ [27].

In the next section some details on the experiment are provided. In order to extract the local susceptibility from the μ^+ Knight shift, the implanted μ^+-position and possible motional state have to be known. This information is deduced from the dephasing rate of the transverse field (TF) μSR-signal. This part of the work is presented in Section 3. Section 4 discusses the Knight shift results, their analysis and interpretation (including previous results on UPd_2Al_3). The conclusion will be that a CEF-model, *i.e.* a local $5f$-electron state provides a consistent picture of our results. Finally, a summary is given in Section 5.

2 Experimental details

The experiments were performed on the surface muon beam line πM3 of the PSI 600 MeV-proton accelerator facility using the general purpose spectrometer GPS in the "veto mode", which suppresses essentially all events not connected with μ^+-stops in the sample, even if the sample is quite small. In our case the monocrystalline UNi_2Al_3 sample had the form of a cylinder with 7.6 mm length and a diameter of 3.2 mm. It was oriented with the cylinder axis (= crystalline a-axis) perpendicular to the μ^+-beam and was attached to the target holder by an essentially massless tube made out of mylar foil so that in effect only the sample produced good muon decay positrons. The positrons were recorded in the three detector telescopes placed above, below and sideways of the sample in a plane transverse to the μ^+-beam. Generally the transverse field (TF) μSR-technique [28] was applied, *i.e.*, the Larmor precession of the μ^+ was observed. The external field (5 mT−0.6 T) was oriented parallel to the incoming μ^+ beam and the incoming μ^+-spin polarization was turned towards a perpendicular orientation by means of a spin rotator. The sample was located inside a He-flow cryostat which allowed to set temperatures between 2 K and 300 K. The sample could be rotated around the cylinder axis (= a-axis) so that the external field **B** could be rotated in the (c,b^*)-plane. For the Knight shift determination $|\mathbf{B}|$ was either precisely measured by an NMR-magnetometer or, replacing the UNi_2Al_3 sample by a small silver plate, by measuring the μ^+-Larmor precession frequency ω_μ in Ag. Since the μ^+ Knight shift in Ag

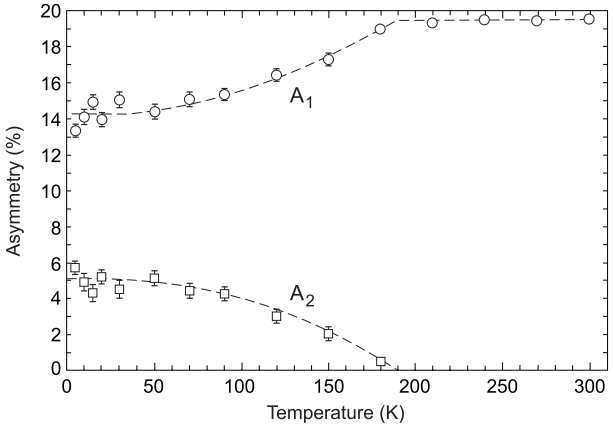

Fig. 1. Temperature dependence of the two amplitudes (asymmetries) A_1 and A_2 for $\mathbf{B} \perp c$-axis ($B = 0.6$ T). The same results are obtained for $\mathbf{B} \parallel a$-axis and different B.

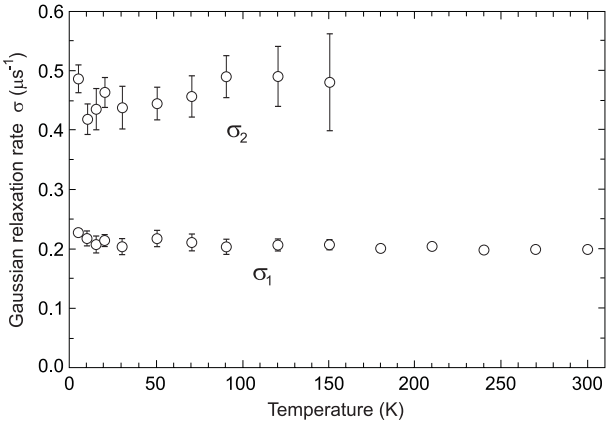

Fig. 2. Temperature dependence of the decay constants σ_1 and σ_2 for $\mathbf{B} \perp c$-axis.

is known ($\sim$ 94 ppm [24]) one can extract from ω_μ the applied field to an accuracy of a few ppm.

The single crystal sample was prepared by the Czochralski method using a tri-arc furnace, the detailed description is given in reference [16]. Resistivity measurements showed the onset of superconductivity at $\sim$ 1 K. μSR test-runs in zero field (ZF) below $T_N = 4$ K showed that the sample was indeed in the magnetically ordered state by showing the appropriate oscillating signal [25].

3 Relaxation rates and muon sites

3.1 Results

The transverse-field (TF) μSR-signal was found to be composed of two distinct components below 200 K, while above 200 K only one component remained. Correspondingly, the time evolution of the spin polarization of the implanted muon ensemble, $P(t)$, was best fitted by the function

$$P(t) = \sum_{i=1}^{2} A_i \exp(-\frac{1}{2}\sigma_i^2 t^2) \cos(\omega_i t + \varphi), \qquad (3.1)$$

where $\omega_i = \gamma_\mu B_{\mu,i}$ are the Larmor frequencies in the local fields $B_{\mu,i}$. The Gaussian decay functions with decay constants σ_i account for the dephasing of the precessing muons due to a field spread around the average $B_{\mu,i}$ (inhomogeneous line broadening). The amplitudes A_i are measures of the relative number of muons contributing to the two components. The fits, performed simultaneously in all three histograms associated with the three positron telescopes, yielded a temperature dependence of the A_i, which is shown for $\mathbf{B} \perp c$-axis ($B = 0.6$ T), as a typical example, in Figure 1. Clearly, the second, always smaller component has died out above 200 K. This component has not been seen in UPd_2Al_3, but it seems to be typical for UNi_2Al_3 since it has also been observed in some previous preliminary studies on another single crystal of different origin [29]. The fact that the relaxation of the two components was best fitted by a Gaussian decay function and, moreover, that the σ_i appeared temperature independent (as an example see Fig. 2) implies that no long range diffusion of the μ^+ takes place. The σ_i thus represent the width of some static Gaussian field distribution which can only be associated with the Al nuclear magnetic moments, the only source of fields which are static on the scale of the μ^+ lifetime in the paramagnetic state of UNi_2Al_3. (The only other moment carrying isotope is ^{61}Ni which, however, has a very low abundance of 1,2% and can be neglected.) As can be seen from Figure 2, σ_2 is about a factor of 2 larger than σ_1.

With the aim to identify the μ^+ positions associated with the two components we have measured the orientation and field dependence of $\sigma_i = \sqrt{M_{2,i}}$, where $M_{2,i}$ are the second moments of the field distributions experienced by the μ^+. We concentrate mainly on the data taken above 200 K which are easier to analyze (only one component) and yield more precise information. Below we present the results, their interpretation will be discussed in the next subsection.

Figure 3 shows the orientation dependence of σ_1 when rotating B in the (c, b^*)-plane for low (10 mT) and high (0.6 T) applied field. The pronounced difference in behavior is known to be the result of quadrupolar interaction of the ^{27}Al-nuclei ($I = 5/2$, $Q = 0.15$ barn) [30]. In the limit when the Zeeman interaction of the Al-nuclear magnetic moment is much larger than the quadrupolar interaction, $M_2(\theta, \phi)$ is given by the well known van Vleck formula [31]. The transition from the dominating quadrupolar regime to the van Vleck regime was followed by measuring the field dependence of σ_1 for the three orientations $B \parallel c$-axis ($\theta = 0°$), $B \parallel b$-axis ($\theta = 90°$) and the $\theta = 45°$ position in between, and always $\phi = 90°$. The results are shown in Figures 4. Finally Figure 5 displays the orientation dependence of σ_2 in high field measured at 5 K. The latter values are not very precisely determined due to the small asymmetry of the second component.

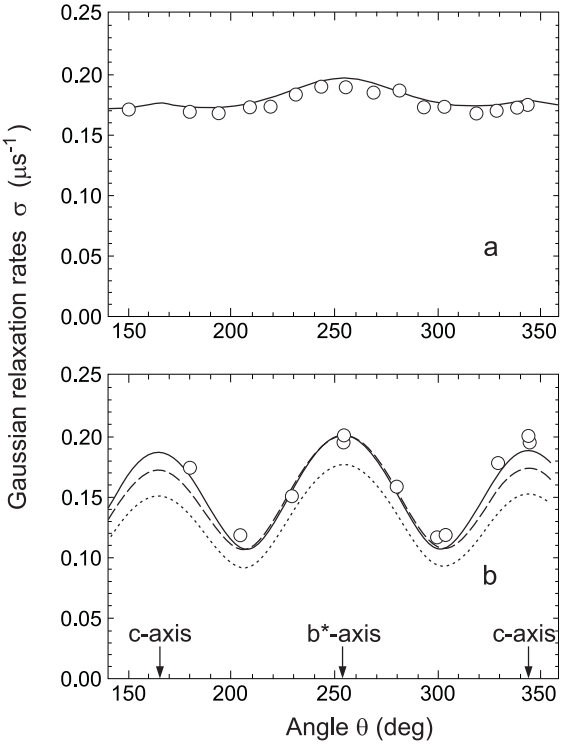

Fig. 3. Dependence of σ_1 on the orientation of the external **B** in the (b^*, c)-plane. (a) $B = 10$ mT, (b) $B = 0.6$ T. The solid lines are the calculated curves for a tunneling μ^+-state extended over six m-sites at a distance of $l = 0.8$ Å from the b-site. The dashed line represents a calculation for the b-site and the dotted line for a static m-site occupation (see text).

3.2 Determination of the muon sites

The interstitial position of the highest $(6/mmm)$ symmetry for space group D^1_{6h} is site b (using Wyckoff's notation), lying at the center of the Al hexagons and situated midway between two U atoms of a vertical U chain (see Fig. 6). This site is found to be occupied by the μ^+ in UPd_2Al_3 [32] but, as shown below, this is not the case for UNi_2Al_3. Therefore, in order to find the muon site in UNi_2Al_3, other interstitial sites with lower symmetry have to be considered.

Within the Al planes and apart from the b-site, the μ^+ can occupy either m- or k-sites of symmetry C_{2v}, or d-sites with D_{3h} site symmetry. The family of six equivalent m-sites, situated on the bisector lines between neighbouring Al atoms at a distance l from the b-site, are obtained by rotations of the point $(x, 2x, 1/2)$ about the hexad axis $(l/a = 2x/\sqrt{3})$ (the coordinates are defined as usual in the crystal frame); the b-site is the particular m-site for $x = 0$, and for $x = 1/3$ or $2/3$ one has the two d-sites midway between two Ni atoms. Similarly, the family of k-sites is generated by sixfold rotations of the point $(x, 0, 1/2)$; a rotation by 30° brings the set of six k-sites into a set of m-sites. As to the interstitial positions outside the Al plane (like sites o, i, f, h), these can be excluded as majority muon sites: for the μ^+ at an o, i or f site one should have a sizeable threefold splitting of the TF-μSR signal

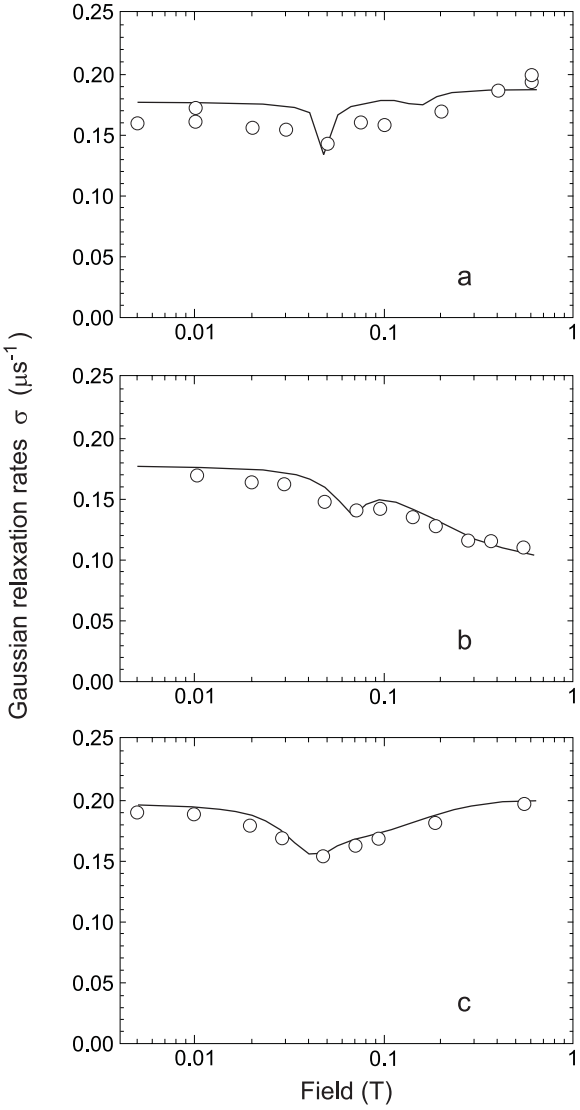

Fig. 4. Field dependence of σ_1 at 295 K for different field directions: (a) $\mathbf{B} \parallel c$-axis, (b) $\widehat{(\mathbf{B}, \mathbf{c})} = 45°$, (c) $\mathbf{B} \perp c$-axis. The solid lines are predictions for an extended μ^+-state with the same optimized position and EFG parameters as in Figure 3 (see text).

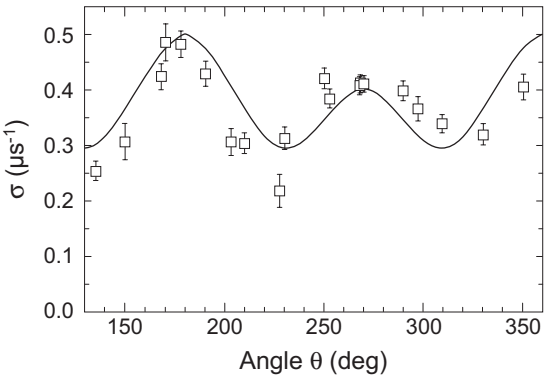

Fig. 5. Dependence of σ_2 on the orientation of **B** ($B = 0.6$ T). The solid line represents a calculation for the d-site. (EFG parameters as in Figs. 3 and 4)

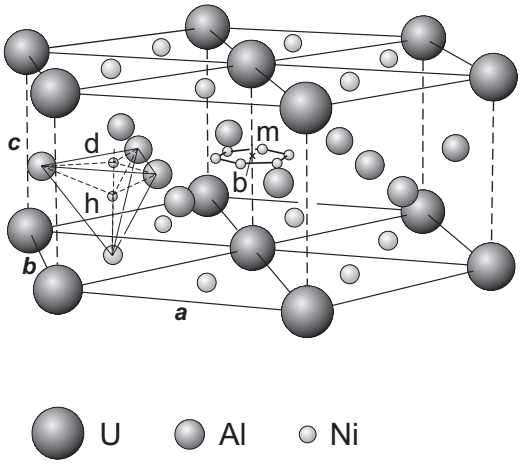

Fig. 6. Crystal structure of hexagonal ($a = b = 5.207$ Å, $c = 4.018$ Å) UNi_2Al_3. Indicated are one of the d-sites and a ring of m-sites comprising the tunneling state. The m-ring is drawn to scale with $\ell = 0.8$ Å (ℓ = distance between two neighboring m-sites; it is essentially also the radius of the m-ring).

due to different Knight shifts which is not seen in the experiment, and no consistent explanation of the data by assuming h as majority μ^+ site could be found either.

The definition of the m (and k) sites contains the continuous parameter x, and to find the actual position $\mathbf{R}_\mu$ of the μ^+ site, the analysis of the angular dependent (Gaussian) relaxation rates $\sigma(\theta, \phi; B)$ is needed. Here θ is the polar angle of $\mathbf{B}$ in the crystal frame (with the z-direction along the c-axis); the azimuthal angle (measured from the a-axis) was kept fixed at $\phi = 90°$.

As long as the field is sufficiently high for the Zeeman term to dominate in the nuclear Hamiltonians, the *a priori* unknown electric field gradients (EFG) at the nuclei act only as small perturbations in determining σ, the value of which remains near to its 'van Vleck' limit given by a 4th-order polynomial of $\cos\theta$ with coefficients determined only by the μ^+ position. The data for $B = 0.6$ T, plotted in Figure 3b, show this high field regime. In the low field limit σ depends quadratically on $\cos\theta$, with coefficients depending strongly on the EFG (Fig. 3a). In the case of UNi_2Al_3 the cross-over from low to high field regimes occurs around ≈ 0.1 T, as seen in Figures 4 where field runs at various fixed crystal orientations are plotted.

In Figure 3b, the measured high-field data for $\sigma(\theta, \phi = 90)$ at $T = 295$ K, $B = 0.6$ T are compared to the predictions for different interstitial μ^+ sites. In calculating these theoretical curves a given set of EFG parameters was used (see below), determined from fitting the low and medium field data. However, σ at the high field $B = 0.6$ T is rather insensitive to this choice, being essentially determined by the μ^+ position alone. The calculations are plotted for the b-site, for a static occupation of m-sites with the best fit value of the position ($l = 0.46$ Å), and for an extended, 'tunneling' or tight binding μ^+ quantum state [33] comprising six equivalent m-sites, with the optimum value $l = 0.8$ Å for this case.

One sees that the calculated σ values for the b site are overall too small. For the static m-sites (with equal occupation of the six equivalent positions) the agreement is better, but the calculated ratio $\sigma(0)/\sigma(90)$ is too low, even for the best value of $l = 0.46$ Å found for this case. Also, there is a theoretical argument against localization of the muon on individual m-sites with such small value of l. Since any potential barrier for the μ^+ between neighbouring m-sites should disappear continuously at site b, it must be already low for $l/(a/2) = 0.46/2.6 \ll 1$, in addition to the fact that the distance 0.46 Å separating the two sites is smaller than the bond length in a H_2 molecule. This makes it plausible that the muon easily 'tunnels' over to neighbouring sites, its wavefunction extending over the ring of the six equivalent m-sites. In fact, the best fit to the data is obtained by the extended state, for the still quite small value of 0.8 Å for l.

We note that the dipolar fields for the extended μ^+ wave functions are, for small l, little affected whether the six maxima are at the m- or k-interstitial positions. In fact, $\sigma(\theta)$ in Figure 3b can equally well be reproduced by assuming the muon localized at the k-sites on the same ring, distinguishing between these two sites on the basis of $\sigma(\theta)$ is, for this small value of l, not possible.

It remains to show that the 'tunneling' μ^+ wave function with the above value of l is also consistent with the data measured in medium and low magnetic fields. In this regime, the value of σ cannot even approximately be determined without the knowledge of the eigenvalues and principal axes of the EFG tensors F_{ik} at the nuclear sites.

Due to their low (orthorhombic) site symmetry, the Al nuclei are subjected to an inherent 'crystal' field gradient F even in the absence of μ^+, observed indeed in NMR experiments [8]. This EFG is then substantially modified in the neighbourhood of the additional point-charge μ^+. A simple but plausible approximation is to assume additivity of the EFG's of different origin, $F = F(\mathrm{cr}) + F(\mu)$, where $F(\mathrm{cr})$ is the 'crystal' contribution (as given by [8]) and $F(\mu)$ is the muon-induced axial-symmetric term, derived from a Coulomb potential $\alpha e/|\mathbf{r} - \mathbf{R}_\mu|$, with α as a free parameter to be found from a fit to our experimental data.

By site symmetry, one principal axis of $F(\mathrm{cr})$ is parallel to the c-axis and a second is along the line connecting the nucleus with the b-site (the third is orthogonal to these two). The published values [8] $\nu_\mathrm{Q} = 799$ kHz for the quadrupolar frequency and $\eta = 1/3$ for the asymmetry parameter determine the eigenvalues f_i of $F(\mathrm{cr})$ as $f_a = -f_c/3$, $f_b = -2f_c/3$, $ef_c = \pm 14.7$ eV/Å^2 (the positive sign was taken here). We used these NMR data for $F(\mathrm{cr})$ as input. As to $F(\mu)$, the medium and low field data shown in Figures 4 and 3a were well reproduced by $\alpha = 7.0$, implying $eF(\mu)_{zz} = -11.4$ eV/Å^2 at the Al nuclei. The theoretical curves shown in Figures 3 and 4 are calculated using these values for $F(\mathrm{cr})$ and $F(\mu)$. (For the Al^{3+} ion perturbed by a single point charge, an earlier calculation [34] gave $\alpha = 3.6$.) The orientation dependence of σ at the lowest field $B = 10$ mT is shown in Figure 3a.

The overall good agreement of both high and low field data for $\sigma_1(\theta)$ with the calculated curves for the μ^+

in a six m-tunneling state on a ring around the b site allows us to conclude that this is the correct site assignment. The tunneling configuration is drawn to scale in Figure 6.

Considering now a possible site for the minority components, the much larger values of σ_2 indicate that the μ^+ site responsible for this signal lies closer to its Al neighbours. Site d has this property, but also the continuum of h-sites given by (1/3, 2/3, z) or (2/3, 1/3, z) if only $(z-1/2) \ll c$ (the d-site is at $z = 1/2$, see Fig. 6). The angular dependence of σ_2 for $B = 0.6$ T is shown in Figure 5 where, besides the data points, the theoretical curve for the d-site is drawn. Since the distance of the muon in a d-site from the nearest three Al nuclei (1.5 Å) is shorter and the role of lattice relaxation is thereby more important than for the m-sites near b, the calculation is given for a radial outwards displacement of the three Al atoms by 10 percent of the μ^+-Al distance. The overall agreement is satisfactory, and we conclude that the minority μ^+ particles are located either at the d-site, or nearby h-sites with $(z - 1/2) \ll c$ close to the basal plane. This assignment is also consistent with the Knight shift results (see Sect. 4). We notice that the small ratio of the amplitudes $A_2/A_1 \approx 1/2$ even at low temperatures imply a suppressed occupation of the minority sites (there are *a priori* two d-sites and only one m-ring state for a given x per unit cell), indicating that the majority site is energetically favoured.

4 Muon Knight shift - evidence for CEF effects in the magnetic response

4.1 Knight shift and magnetic susceptibility

The Knight shift of interstitially implanted μ^+ in a metal consists of two contributions: (i) dipolar fields from field-induced moments in the neighborhood of the μ^+, (ii) a contact hyperfine field arising from a field induced local spin polarization at the μ^+ position carried by conduction electrons.

The magnetic response of an intermetallic system containing rare earth or actinide ions is mainly associated with the $4f$ or $5f$-electrons present. It is strongly temperature dependent and for non-cubic systems of tensorial form. In addition, the conduction electron system may contribute a temperature independent and isotropic (Pauli like), generally quite small, term. We may thus write the total susceptibility tensor as

$$\overleftrightarrow{\chi}_{\rm tot} = \chi_0 \overleftrightarrow{E} + \overleftrightarrow{\chi}_f, \tag{4.1}$$

where $\overleftrightarrow{E}$ is the unit tensor. The moment induced by an external field $\mathbf{B}$ on the f-electron atoms is given by

$$\boldsymbol{\mu}_f = \overleftrightarrow{\chi}_f \cdot \mathbf{B}, \tag{4.2}$$

which leads to a dipolar term in the μ^+-Knight shift [25]:

$$K_{{\rm dip},f} = \mathbf{b} \cdot \overleftrightarrow{A}_{\rm dip} \cdot \overleftrightarrow{\chi}_f \cdot \mathbf{b}, \tag{4.3}$$

where $\mathbf{b} = \mathbf{B}/B$, and $\overleftrightarrow{A}_{\rm dip}$ is a dipolar coupling tensor which depends on the crystal structure and the μ^+-site and can be easily calculated. Further ${\rm Tr}(\overleftrightarrow{A}_{\rm dip}) = 0$. *Via* the RKKY-interaction the induced moments will also induce a spin polarization in the conduction electron system, which shows the famous oscillatory behavior as one moves away from the f-electron atom. The resulting spin polarization at the μ^+-position produces a contact hyperfine field which contributes to the muon Knight shift *via* the expression

$$K_{{\rm c},f} = A_{\rm c} \mathbf{b} \cdot \overleftrightarrow{E} \cdot \overleftrightarrow{\chi}_f \cdot \mathbf{b}, \tag{4.4}$$

assuming an isotropic RKKY-mechanism.

The small conduction electron susceptibility will give rise to a correspondingly small, temperature independent and isotropic further contribution to the Knight shift

$$K_0 = A_0 \chi_0. \tag{4.5}$$

Hence in total we will have

$$K_{\rm tot} = K_0 + K_{{\rm c},f} + K_{{\rm dip},f}. \tag{4.6}$$

For a system with axial symmetry, like that of U in hexagonal UNi_2Al_3, $\overleftrightarrow{\chi}_f$ will be given by

$$\overleftrightarrow{\chi}_f = \begin{pmatrix} \chi_\perp & 0 & 0 \\ c & \chi_\perp & 0 \\ c & 0 & \chi_\parallel \end{pmatrix} \tag{4.7}$$

where $\parallel$ refers to $\mathbf{B}$ parallel to the c-axis and $\perp$ to $\mathbf{B}$ perpendicular to the c-axis. As remarked above the dipolar coupling tensor depends on the assumed μ^+-site and its point symmetry. The point symmetry of the m-site in UNi_2Al_3 is represented by the point group $mm2$. The dipolar coupling tensor has the general form

$$\overleftrightarrow{A}_{\rm dip} = \begin{pmatrix} A_{xx} & A_{xy} & 0 \\ A_{xy} & A_{yy} & 0 \\ 0 & 0 & A_{zz} \end{pmatrix}, \quad {\rm Tr}(\overleftrightarrow{A}_{\rm dip}) = 0 \tag{4.8}$$

with

$$\begin{aligned} A_{xx} &= \cos^2\varphi A_\xi + \sin^2\varphi A_\eta \\ A_{yy} &= \sin^2\varphi A_\xi + \cos^2 A_\eta \\ A_{zz} &= A_z \\ A_{xy} &= \sin\varphi\cos\varphi(A_\eta - A_\xi), \end{aligned} \tag{4.9}$$

where A_i are the principal values of $\overleftrightarrow{A}_{\rm dip}$ and φ is the angle between the principal axis ξ and a fixed crystal axis x, *i.e.* the a-axis. The three magnetically inequivalent m-sites correspond to $\varphi = 0°$, 60° and 120°. The identified tunneling state of the μ^+ over six m-sites (or k-sites) around the b-site implies that the effective dipolar coupling tensor has to be averaged over the magnetically inequivalent m

(or k)-sites in this set. Again, there are three, each appearing twice. The average has the diagonal and axially symmetric form

$$\langle \overleftrightarrow{A}_{\rm dip} \rangle = \begin{pmatrix} \frac{1}{2}(A_\xi + A_\eta) & 0 & 0 \\ 0 & \frac{1}{2}(A_\xi + A_\eta) & 0 \\ 0 & 0 & A_z \end{pmatrix}, \qquad (4.10)$$

which corresponds to the dipolar coupling tensor for the b-site, the point symmetry of which is D_{6h}. This was to be expected since the μ^+-tunneling wave function, centered at the b-site, has the same symmetry. Using the exact positions of the m-sites connected by the tunneling state ($x = 0.0877$), we calculate

$$\frac{1}{2}(A_\xi + A_\eta) = -\frac{1}{2}A_{\rm dip} = -0.1377 \text{ T}/\mu_{\rm B},$$

$$A_z = A_{\rm dip} = +0.2755 \text{ T}/\mu_{\rm B}.$$

(The same values are obtained for a tunneling state over six k-sites.)

These results imply that all μ^+ in the tunneling state exhibit a unique Knight shift, *i.e.*, no splitting of the TF-μSR signal should occur. Further, when rotating **B** in the basal plane the Knight shift will stay constant. Rotating **B** around, say, the a-axis, a single $\cos^2\theta$-dependence of the Knight shift will result.

The same is true for the d-site ($z = 0.5$) for which one calculates $A_{xx} = A_{yy} = -\frac{1}{2}A_{zz} = 0.003\frac{\rm T}{\mu_{\rm B}}$, $\quad A_{i\neq j} = 0$. As can be seen the dipolar coupling strength is significantly smaller than for the m-site tunneling state.

The total Knight shift perpendicular and along the c-axis assumes now the simple form

$$K_\perp = K_0 + (A_{\rm c} - \frac{1}{2}A_{\rm dip})\chi_{f,\perp},$$

$$K_\parallel = K_0 + (A_{\rm c} + A_{\rm dip})\chi_{f,\parallel}, \qquad (4.11)$$

with

$$\chi_{f,\perp} = \chi_{\perp,\rm tot} - \chi_0,$$

$$\chi_{f,\parallel} = \chi_{\parallel,\rm tot} - \chi_0.$$

4.2 Experimental results

All Knight shift data were obtained in an external field of 0.6 T. Angular scans served to search for a line splitting and the type of angular dependence. Rotating **B** in the basal plane no anisotropy was observed, while a $\cos^2\theta$-dependence was seen when rotating **B** in the (b^*, c)-plane (see Fig. 7), in agreement with the expectations. As can be seen, the anisotropy of the minority signal at 5 K is much smaller than that of the majority signal, consistent with the small $A_{\rm dip}$ for the d-site. From now on we will only consider the majority Larmor frequency.

Figure 8 displays the temperature dependence of the precession frequency for **B** $\parallel$ c-axis and for **B** $\perp$ c-axis.

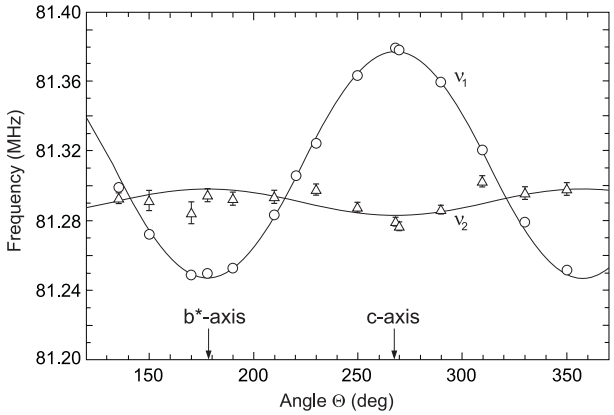

Fig. 7. Dependence of the precession frequencies ν_1 and ν_2 on the orientation of **B** in the (b^*, c)-plane at 5 K. The solid lines represent $\cos^2\theta$ fits. The unshifted frequency in the external field (0.6 T) is 81.3103 MHz.

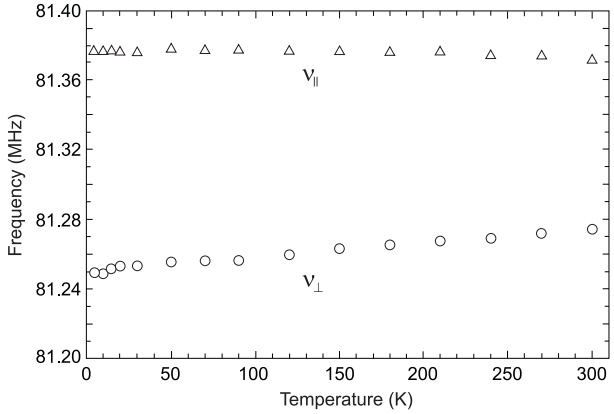

Fig. 8. Temperature dependence of the precession frequencies for **B** $\parallel$ c-axis and **B** $\perp$ c-axis ($B = 0.599935$ T).

The total relative frequency shift with respect to the applied field ($\nu_0 = (\gamma_\mu/2\pi)B$) contains, besides the Knight shift, contributions from the Lorentz field and the demagnetization field, *i.e.*

$$\frac{\Delta\nu}{\nu_0} = \frac{\nu - \nu_0}{\nu_0} = K_{\rm tot} + \left(\frac{4\pi}{3} - N\right)\chi_{\rm tot}, \qquad (4.12)$$

where N is the demagnetization factor (tensor) and $\chi_{\rm tot}$ the total bulk susceptibility in emu/cm^3. The cylindrical sample (cylinder axis = a-axis) has a diameter to length ratio of 3.2/7.6. The applied field **B** is always directed perpendicular to the cylinder axis. Using the tables in reference [35] we estimate $N/4\pi \simeq 0.445$. The bulk susceptibility is taken from [16]. The extracted total Knight shift is plotted in Figure 9 *versus* the bulk susceptibility for both **B** $\parallel$ c-axis and **B** $\perp$ c-axis (Clogston-Jaccarino plot). According to equations (4.11) a linear scaling of $K_{\rm tot}$ with χ_f is expected to show up. Indeed for **B** $\perp$ c-axis for $T \geq 150$ K a scaling is clearly visible which allows to fit the slope: $(A_{\rm c} - \frac{1}{2}A_{\rm dip}) = (0.324 \pm 0.061)$ kG/$\mu_{\rm B}$. For **B** $\parallel$ c-axis it is difficult to determine the slope. In any case, below 150 K the scaling is lost altogether. To

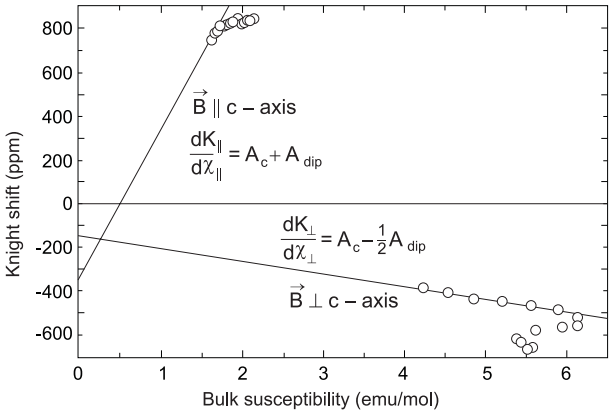

Fig. 9. Plot of Knight shift versus bulk susceptibility (Clogston-Jaccarino plot). The line with the negative slope ($B \perp c$-axis) represents a linear fit to the six points with $T >$ 120 K. The line with the positive slope (calculated, see text) is shifted horizontally to match the high temperature points for $B \parallel c$-axis. The two lines cross at $K_0 = -(167 \pm 50)$ ppm and $\chi_0 \simeq 0.25(8) \times 10^{-3}$ emu/mol.

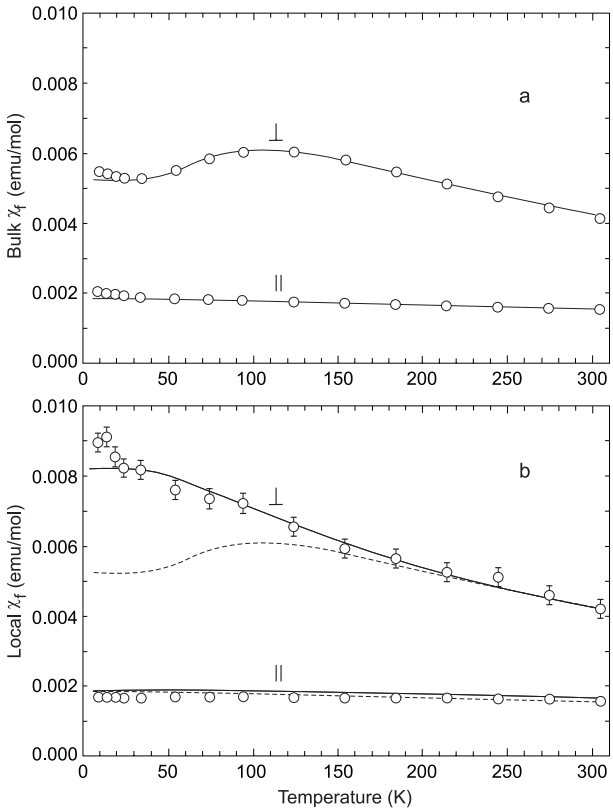

Fig. 10. Temperature dependence of (a) the bulk $5f$-electron susceptibility ($=\overleftrightarrow{\chi}_{\rm tot} - \chi_0$) and (b) the local $5f$-electron susceptibility ($\overleftrightarrow{\chi}_{\rm loc} - \chi_0$) for $\mathbf{B} \perp c$-axis and $B \parallel c$-axis in UNi_2Al_3. The solid lines represent CEF-calculations (see text). For better comparison the calculated line from the upper figure is also reproduced in the lower figure (dashed line).

make use of the $\mathbf{B} \parallel c$-axis data we follow the following procedure. Since we know $A_{\rm dip}$ we can calculate $A_{\rm c}$ from the slope $A_{\rm c} - \frac{1}{2}A_{\rm dip} = -0.324$ kG/$\mu_{\rm B}$: $A_{\rm c} = -(1.054 \pm 0.061)$ kG/$\mu_{\rm B}$. (In UPd_2Al_3 $A_{\rm c} = -1.21(3)$ kG/$\mu_{\rm B}$ [32]), and hence we know the expected slope for $K_\parallel$ *versus* $\chi_\parallel$: $A_{\rm c} + A_{\rm dip} = (3.81 \pm 0.06)$ kG/$\mu_{\rm B}$. Next we construct a line in Figure 9 with the calculated slope and move it parallel to itself such that it passes most closely through the high temperature points ($T > 200$ K) for $\mathbf{B} \parallel c$-axis. This line is shown in Figure 9. We see that the two drawn lines cross at $\chi \simeq (0.28 \pm 0.08) \times 10^{-3} \frac{\rm emu}{\rm mol}$ and $K = -(167 \pm 50)$ ppm. The assigned error bars result from the uncertainties in the slopes. In the spirit of equations (4.11) $\chi = 0.28 \times 10^{-3}$ emu/mol and $K = -167$ ppm are to be identified with the temperature independent K_0 and χ_0. It is hereby assumed that χ_0 and K_0 are isotropic as it is usually believed to be the case. A temperature independent and isotropic contribution of $\chi_0 = 0.28 \times 10^{-3}$ emu/mol is not in conflict with the overall temperature dependence of the bulk susceptibility. In UPd_2Al_3 the corresponding values were found to be $K_0 = -230(60)$ ppm and $\chi_0 = 0.75(5) \times 10^{-3}$ emu/mol [32].

We now address the loss of scaling at lower temperatures. In principle, the relation between Knight shift and susceptibility should still be given by equation (4.12). A loss of scaling may be associated with $A_{\rm c}$ which may become temperature dependent at lower temperature, as has been discussed, for instance, in reference [36]. Secondly, the effective susceptibility may deviate from the bulk susceptibility. Since more than 90% of $\langle \overleftrightarrow{A}_{\rm dip} \rangle$ arises from only the two nearest U-neighbors above and below the ring of $m(k)$-sites, it is in fact the atomic susceptibility of those two U-ions which must become different from the bulk susceptibility. We call it the local susceptibility.

As far as a possible change of $A_{\rm c}$ is concerned, it can be excluded since the Al nuclear Knight shift, which is mainly arising from the RKKY-mechanism, scales with the bulk susceptibility down to 4.2 K [8]. This indicates that the exchange coupling of the conduction electrons with the $5f$-electron state is not changing at lower temperatures. Hence, we conclude that $A_{\rm c}$ is constant over the whole temperature range. It thus seems that the problem lies with the local susceptibility, possibly because of the presence of the μ^+ (see next section). Assuming now that equations (4.11) hold with unchanged $A_{\rm c}$ and $A_{\rm dip}$ (the latter is granted as long as no site-change is involved), we can determine the temperature dependence of the local $5f$-electron susceptibility $\chi_{f,\rm local}$, associated with the two mentioned U-neighbors, over the whole temperature range. The results are plotted in Figure 10b. Figure 10a shows the undisturbed $5f$-electron susceptibility $\chi_f = \chi_{\rm tot} - \chi_0$. Comparing Figures 10a and 10b, one sees that for $\mathbf{B} \parallel c$-axis the local susceptibility follows by and large χ_f, most closely above 200 K. Much more pronounced are the differences for $\mathbf{B} \perp c$-axis. The local susceptibility $\chi_{f,\rm local}$ keeps rising with decreasing temperature and does not reflect the maximum in the susceptibility near 110 K. In fact it can be well fitted by a Curie-Weiss expression in the whole temperature range. Above 150 K the local susceptibility is essentially identical with χ_f.

4.3 On the interpretation of the susceptibilities

A previous study of the μ^+-Knight shift in $PrNi_5$, which has the same hexagonal $CaCu_5$ structure as UNi_2Al_3, found a similar breakdown of the scaling of K with χ_f at low temperatures [26]. In this compound the μ^+ is located at the i-site near the f-site and the TF-signal splits into up to 3 components. The analysis yields a local susceptibility which, in the presence of the μ^+, becomes anisotropic in the basal plane. The axially symmetric bulk susceptibility tensor is well explained on the basis of the CEF-splitting of the $Pr^{3+}-{}^3H_4$ ground state multiplet with a singlet state as the lowest level. The CEF-level splitting is also well established by inelastic neutron scattering [18]. The modified local susceptibility tensor in the presence of the μ^+ is well reproduced by considering a μ^+ induced modification of the CEF-parameters for the nearest Pr-neighbors including a change in symmetry which leads to a non-zero $B_2^2O_2^2$ term in the CEF-Hamiltonian. The excellent agreement between the modified CEF-splitting and the resulting susceptibility with the data in $PrNi_5$ motivates us to try a similar approach for UNi_2Al_3, implying that the $5f$-electrons are sufficiently well localized. As mentioned in Section 1, the anisotropic susceptibility found in UPd_2Al_3 and the behavior of the electronic specific heat could be reasonably well reproduced by adopting a CEF-model and assuming U to be in the tetravalent ionic state with two f-electrons forming the ground state multiplet ${}^3H_4$ with the non-magnetic Γ_4 singlet as the lowest level [15]. In this model the anisotropy of χ_f and in particular the maximum in χ_f for $\mathbf{B} \perp c$-axis is well reproduced [15]. To obtain quantitative agreement one has also to introduce anisotropic molecular field parameters through the equation

$$\frac{1}{\chi_{f,i}} = \frac{1}{\chi_{\mathrm{CEF},i}} + \lambda_i, \quad i = \parallel, \perp, \tag{4.13}$$

where $\chi_{\mathrm{CEF},i}$ is given by the CEF-calculation. Qualitatively the situation is very similar to $PrNi_5$.

An *ab initio* crystal field theory by Richter *et al.* [37], however, failed to reproduce the extracted CEF-parameters for UPd_2Al_3.

Using the appropriate CEF-Hamiltonian

$$\mathcal{H}_{\mathrm{CEF}} = B_2^0O_2^0 + B_4^0O_4^0 + B_6^0O_6^0 + B_6^6O_6^6 \tag{4.14}$$

and the CEF-parameter for UPd_2Al_3 as an initial guess we first tried to reproduce the susceptibility data for UNi_2Al_3. With the adjusted parameters, quoted in Table 1, we find an excellent fit, shown as solid lines in Figure 10a. The CEF-parameters are not very different from those of UPd_2Al_3. The main difference lies in the molecular field constants which are about a factor of 3-4 larger than in UPd_2Al_3. This may in part be due to the somewhat smaller (4%) distance between the two nearest neighbor U-atoms in UNi_2Al_3 as compared with UPd_2Al_3. Also it is generally held that in UNi_2Al_3 the f-electrons may be less localized, *i.e.*, hybridization with the conduction electrons may be stronger, leading to a larger RKKY-type of coupling between the U-ions.

Table 1. Adjusted CEF-parameters for UNi_2Al_3 with and without the μ^+-disturbance. The B_l^m are given in meV, the λ_i in mol/emu.

lattice	B_2^0	B_4^0	B_6^0	B_6^6	$\lambda_\parallel$	$\lambda_\perp$
undisturbed	0.743	4.2×10^{-3}	4.67×10^{-4}	0.011	450	67
with μ^+	0.41	4.0×10^{-3}	5×10^{-5}	0.011	450	67

Next we try to reproduce the modified local susceptibility. Compared to the case of $PrNi_5$ this requires no additional terms in the CEF-Hamiltonian, since the presence of the μ^+ in the tunneling state over $6m$ (or $6k$)-sites does not alter the axial symmetry of the nearest two U-ions position along the c-direction above and below the b-site, even if those ions are somewhat displaced symmetrically away from the μ^+. In addition, the electric field introduced by the screened μ^+ charge is likewise axially symmetric. It can then be shown that the parameter B_6^6 is not influenced by the presence of the μ^+, and we will fix it at the undisturbed value (see discussion in Ref. [27]). Thus, by varying only the parameters B_2^0, B_4^0 and B_6^0, keeping also $\lambda_\perp$ and $\lambda_\parallel$ fixed, it is possible to reproduce the local susceptibility quite well as demonstrated by the solid lines in Figure 10b. The "fitted" parameters are also collected in Table 1. The most drastically affected parameters by the implanted μ^+ are B_2^0 and B_6^0. All derived eigenvalues and eigenfunctions are presented in Table 2. As can be seen, the presence of the μ^+ leaves the Γ_4-singlet as the ground state, but the first excited states is now a Γ_5-doublet slightly lower in energy than the Γ_1-singlet in undisturbed UNi_2Al_3. The analysis in reference [24] for undisturbed UNi_2Al_3 results in the same order of states, but with significantly different energy spacings.

It is now interesting to check whether the measured μ^+-Knight shift in UPd_2Al_3 can be reproduced by the same CEF-approach as well. We take the μSR and bulk susceptibility data from the thesis of Feyerherm [32]. Figure 11a shows the measured bulk susceptibility (corrected for χ_0) and our best CEF-"fit". To arrive at this fit, the calculated χ_{CEF} had to be shifted by -0.002 emu/mol for $B \perp c$-axis and by -0.0005 emu/mol for $\mathbf{B} \parallel c$-axis. The adopted CEF-parameters (somewhat different from those of [15]) are collected in Table 3. Turning to the muon Knight shift we note that it scales very well with the bulk susceptibility down to ~ 25 K and the deviation between χ and K below 25 K is much smaller than in UNi_2Al_3, but clearly present. Figure 11b displays the local susceptibility extracted from the μ^+ Knight shift. Again the changes are very well accounted for by adjusting only B_2^0, B_6^0 and keeping B_4^0, B_6^6 and $\lambda_\perp, \lambda_\parallel$ fixed (see Tab. 3). The diamagnetic corrections are unchanged. The ordering of the energy levels is the same as in UNi_2Al_3. The CEF level splitting is consistent with the analysis in reference [15] and the tentative findings in reference [22].

4.4 Discussion

The absence of well resolved CEF-levels in inelastic neutron scattering (a well known observation in intermetallic U-compounds, the only exception seems to be UPd_3) has

Table 2. CEF-eigenstates and eigenvalues for UNi_2Al_3 with and without the μ^+ disturbance.

level	E (meV) without μ^+	eigenfunctions	E (meV) with μ^+	eigenfunctions
1	0	$\Gamma_4 = \frac{1}{\sqrt{2}}(\|+3\rangle - \|-3\rangle)$	0	$\Gamma_4 = \frac{1}{\sqrt{2}}(\|+3\rangle - \|-3\rangle)$
2	15.6	$\Gamma_1 = \|0\rangle$	13.1	$\Gamma_5 = 0.84\|\pm 2\rangle - 0.54\|\pm 4\rangle$
3	27.9	$\Gamma_6 = \|\pm 1\rangle$	25.8	$\Gamma_1 = \|0\rangle$
4	29.4	$\Gamma_5 = 0.86\|\pm 2\rangle - 0.51\|\mp 4\rangle$	26.2	$\Gamma_6 = \|\pm 1\rangle$
5	55.2	$\Gamma_3 = \frac{1}{\sqrt{2}}(\|3\rangle + \|-3\rangle)$	55.4	$\Gamma_3 = \frac{1}{\sqrt{2}}(\|3\rangle + \|-3\rangle$
6	76.8	$\Gamma_5 = 0.51\|\mp 2\rangle + 0.85\|\pm 4\rangle$	59.4	$\Gamma_5 = 0.54\|\mp 2\rangle + 0.84\|\pm 4\rangle$

Table 3. Adjusted CEF-parameters for UPd_2Al_3 with and without the μ^+-disturbance. The B_l^m are given in meV, the λ_i in mol/emu.

lattice	B_2^0	B_4^0	B_6^0	B_6^6	$\lambda_\parallel$	$\lambda_\perp$
undisturbed	0.8	4×10^{-3}	1.67×10^{-4}	6.9×10^{-3}	150	18
with μ^+	0.625	4×10^{-3}	6.5×10^{-5}	6.9×10^{-3}	150	18

induced researchers to look for alternative explanations of various properties of UPd_2Al_3 (see, *e.g.*, [38]). In addition, the possible coexistence of different types of f-electron states of itinerant and local nature, respectively [10–12], has motivated band structure calculations on the basis of purely itinerant $5f$-electrons [13,23]. To our knowledge, none of these alternative approaches have succeeded in explaining the temperature dependence and anisotropy of the magnetic susceptibility in UPd_2Al_3. Hence, at least phenomenologically, the CEF-calculations provide so far the best theoretical model.

The important observation following from our μSR study is the fact that the presence of the μ^+ obviously modifies the magnetic response of the nearest U-neighbors, both in UPd_2Al_3 and UNi_2Al_3 at low T, while the Al-nuclear Knight shift reflects the bulk susceptibility down to the magnetic ordering temperatures. Any explanation of the magnetic susceptibility must be able to account also for the observed μ^+ induced changes. The most obvious changes brought about by the presence of the μ^+ are a certain local lattice relaxation, well known from hydrogen in metals studies, and a modified conduction electron distribution due to the set up of an electron cloud around the μ^+, screening its positive charge. Both effects will change locally the crystal field properties, in particular, if the lattice relaxation leads also to a lowering of the local point symmetry. This has been amply demonstrated by the μSR-studies in $PrNi_5$ [26] and more recently in cubic $PrIn_3$ [27]. It is difficult to see how, *e.g.*, an itinerant f-electron system can be affected by a single μ^+. The more Curie-Weiss like behavior of the local susceptibility in UNi_2Al_3 for $\mathbf{B} \perp c$-axis at low T could, *e.g.*, imply a localization of the $5f$-electrons at the μ^+ nearest neighbor U-ions. Whether this is a viable possibility is questionable. The CEF-approach, however, is appealing since it leads to a consistent and plausible explanation of both the intrinsic and μ^+-modified local susceptibilities.

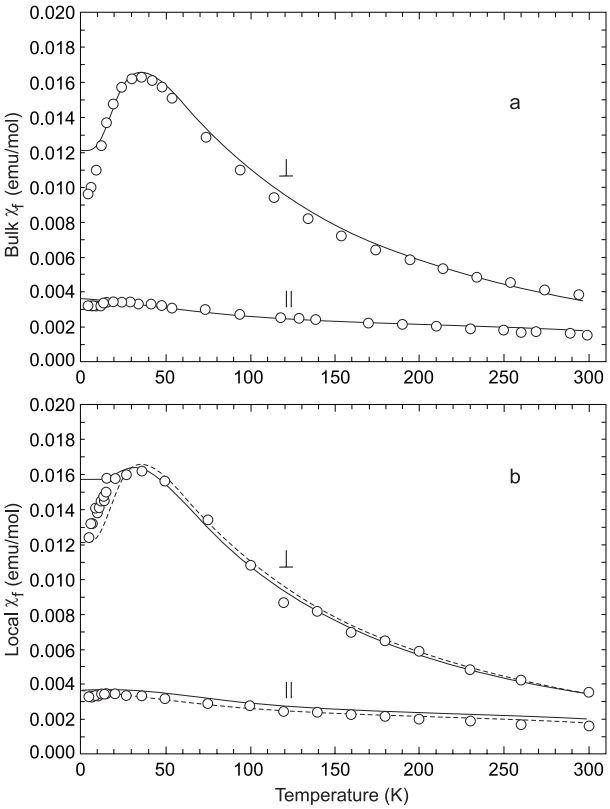

Fig. 11. Bulk $5f$-electron and local $5f$-electron susceptibility in UPd_2Al_3. See caption of Figure 10. The solid lines represent again CEF-calculations (see text).

Comparing Tables 1 and 3 we see that in both systems the B_l^0 parameters are modified in the same directions, *i.e.*, all are reduced. It is tempting to ascribe the reduction to the crystal electric field arising from the screened μ^+, assuming the intrinsic CEF to be unchanged. However, a simple point charge model fails to account for the reductions. Considering the difference between UPd_2Al_3 and UNi_2Al_3 one has also to take into account the different μ^+-sites (b-site *versus* the tunneling state over six m (or k)-sites).

The μSR results are consistent with the observation that doping of UPd_2Al_3 with hydrogen shifts the magnetic susceptibility towards a Curie-Weiss behavior with increasing hydrogen content (maximum 1.3%) [39].

The μSR results demonstrate that already a single μ^+ (infinite dilute hydrogen limit) can produce this result.

We are left with the problem to understand the success of the CEF-approach in view of the weak direct evidence for a CEF-splitting of the $5f$-electron state. We suggest that it is related to lifetime effects, which broaden the CEF-levels considerably, but not to the extend that the CEF-level splitting breaks down completely. This will be studied in future work.

It is also interesting to have a look at the other extracted parameters: A_c, K_0 and χ_0. The A_c from the two compounds are rather similar. Since in a RKKY-picture $A_c \propto J_0$, where J_0 is the exchange coupling constant between the conduction electrons and the local f-electrons, it seems that the J_0 are not very different for the two compounds. This is inconsistent with the very different molecular field constants λ which, if arising from the same RKKY interaction, should scale with J_0^2. Moreover, the anisotropy of λ suggests a more complex behavior requiring an anisotropic exchange mechanism, at least as far as the U-ions are concerned. There is no evidence in the data that A_c could be anisotropic.

Perhaps not unrelated is the question about the validity of our assumption that K_0 has to be isotropic. This assumption leads to a rather large isotropic and temperature independent χ_0 which, at least in the case of UPd_2Al_3, seems to be inconsistent with the temperature dependence of the bulk susceptibility (in particular with $\chi_\parallel$ (T)). If, instead, we admit $\chi_0 = 0$, we find that both $\chi_{\mathrm{local},\parallel}$ and $\chi_{5f,\parallel}$ can be slightly better reproduced by the CEF-calculations. It reduces also the diamagnetic corrections, needed to obtain perfect agreement in the case of UPd_2Al_3. This affects the fitted CEF-parameters insignificantly, but shifts the molecular field parameters to slightly reduced values.

Finally, from the present results in UNi_2Al_3 we cannot provide a clue regarding the coexistence of local and itinerant states of $5f$-character. If existing, probably with similar magnetic form factors, the functional form of the temperature dependence of the magnetic response of both states cannot be much different in order to be consistent with the data. Polarized neutron scattering on UPd_2Al_3 was claimed to show a rather large conduction electron spin polarization of 12% of the total magnetization in the easy plane at 36 K [20]. We should have noticed this effect (which would contribute several +100 ppm to $K_\perp$ in UNi_2Al_3) if the temperature dependence of the spin polarization were much different from $\chi_{\mathrm{tot},\perp}$(T). Otherwise it may contribute to A_c and would be indistinguishable from the RKKY-contribution. Hence, it would be very interesting to know the temperature dependence of the induced conduction electron polarization.

5 Summary

Implanted positive muons in UNi_2Al_3 are found at two different interstitial sites: the very unusual d-site ($(\frac{1}{3}\ \frac{2}{3}\ \frac{1}{2})$ and equivalent positions) and in a tunneling state over six m (or k)-sites forming a ring around the b-site ($0\ 0\ \frac{1}{2}$). Note that in UPd_2Al_3 the μ^+ resides at the b-site [11]. The population of the d-site ($\sim 30\%$ at low T) decreases with rising temperature and becomes zero above 200 K. The population of the tunneling state rises by the same proportion, it is the only μ^+-state above 200 K. From the field dependence of the TF-relaxation rates the electric field gradients at the nearest Al-nuclei could be evaluated. They consist of an intrinsic contribution, as also found in NQR-measurements [8], and a μ^+ induced radially directed term. The determination of the anisotropic Knight shift of the majority component constitutes the main result of the present work. It scales well with the bulk susceptibility above 150 K but in the basal (easy) plane the scaling is lost below 150 K. In particular, the shallow maximum in the bulk susceptibility at ~ 110 K is not seen in the Knight shift which continues to rise with decreasing temperature. For $B \parallel c$-axis the μ^+ Knight shift shows as little temperature dependence as the bulk susceptibility. Knowing the μ^+-sites (simultaneous occupation of the six m (or k)-sites around the b-site) and therefore the dipolar coupling tensor $\langle \overleftrightarrow{A}_{\mathrm{dip}} \rangle$ associated with the two nearest U-neighbors along the c-direction (more distant U-neighbor contribute negligibly to $\overleftrightarrow{A}_{\mathrm{dip}}$) we could extract the local (atomic) susceptibility of the two nearest U-neighbors. Motivated by previous work on $PrNi_5$, which has the same hexagonal ($CaCu_5$) crystal structure as UNi_2Al_3 and which showed a similar modification of the local susceptibility in the presence of the μ^+ [26], we tried to reproduce the anisotropy and the temperature dependence of both the bulk susceptibility and the local susceptibility by a CEF-model. This had been done before for undisturbed UPd_2Al_3 and UNi_2Al_3, assuming the uranium to be in the tetravalent (U^{4+}) state with the configuration $5f^2\ ^3H_4$ [15,24] which is equivalent to the Pr^{3+}-state in $PrNi_5$. The presence of the μ^+ does not alter the axial symmetry of the nearest neighbor U-positions above and below the b-site so that the CEF-Hamiltonian keeps its hexagonal form and only the parameters B_2^0, B_4^0 and B_6^0 can be affected by the μ^+. An excellent description of both data sets was achieved. Reanalyzing previously obtained data on UPd_2Al_3 in the same way, again excellent consistency was found. The important point here is that the disturbance induced by the presence of the μ^+ is used to test the possible mechanism responsible for the observed magnetic response. The most obvious consequence following from the implantation of the positively charged muon is a change in the local CEF-properties which are caused by the additional electric field arising from the screened μ^+-charge and, more indirectly, also by an induced lattice relaxation altering the symmetry conditions and the intrinsic CEF. The magnetic coupling between the U-ions does not seem to be affected by the μ^+ since the Néel temperatures are not changed and also the molecular field parameters λ remain the same. From all this we conclude that the excellent description of both the bulk susceptibility and the modified local susceptibility within a CEF-picture is not fortuitous but rather implies the validity of this picture. Hence, it appears that both UPd_2Al_3 and UNi_2Al_3 can be viewed as possessing rather

localized $5f$-electron states. Whether in addition some itinerant states of f-character exist cannot be decided by the present work. The absence of a well developed and resolved CEF-splitting in inelastic neutron work remains to be an enigma.

References

1. C. Geibel, S. Thies, D. Koszorowski, A. Mehnar, A. Grauel, B. Seidel, U. Ahlheim, R. Helfrich, K. Petersen, C.D. Bredl, F. Steglich, Z. Phys. B **83**, 305 (1991).
2. C. Geibel, C. Schank, S. Thies, H. Kitazawa, C.D. Bredl, A. Böhm, M. Rau, A. Grauel, R. Caspary, R. Helfrich, U. Ahlheim, G. Weber, F. Steglich, Z. Phys. B **84**, 1 (1991).
3. A. Krimmel, P. Fischer, B. Roessli, H. Maletta, G. Geibel, C. Schank, A. Grauel, A. Loidl, F. Steglich, Z. Phys. B **86**, 161 (1992).
4. N. Sato, N. Aso, G.H. Lander, B. Roessli, T. Komatsubara, Y.Endoh, J. Phys. Soc. Jap. **66**, 1884 (1997); *ibid.* **66**, 2981 (1997); N. Bernhoeft, N. Sato, B. Roessli, N. Aso, A. Hiess, G.H. Lander, Y. Endoh, T. Komatsubara, Phys. Rev. Lett. **81**, 4244 (1998).
5. N. Metoki, Y. Haga, Y. Koike, N. Aso, Y. Ōnuki, J. Phys. Soc. Jap. **66**, 2560 (1997).
6. J.G. Lussier, M. Mao, A. Schröder, J.D. Garrett, B.D. Gaulin, S.M. Shapiro, W.J.L. Buyers, Phys. Rev. B **56**, 11749 (1997).
7. N. Sato, N. Aso, N. Tateiwa, N. Koga, T. Komatsumara, N. Metoki, Physica B **230-232**, 367 (1997).
8. M. Kyogaku, Y. Kitaoka, K. Asayama, C. Geibel, C. Schank, F. Steglich, J. Phys. Soc. Jap. **62**, 4016 (1993).
9. H. Tou, Y. Kitaoka, T. Kamatsuka, K. Asayama, C. Geibel, F. Steglich, S. Süllow, J.A. Mydosh, Physica B **230-232**, 360 (1997).
10. R. Caspary, P. Hellmann, M. Keller, G. Sparn, C. Wassilew, R. Köhler, C. Geibel, C. Schank, F. Steglich, N.E. Phillips, Phys. Rev. Lett. **71**, 2146 (1993).
11. R. Feyerherm, A. Amato, F.N. Gygax, A. Schenck, C. Geibel, F. Steglich, N. Sato, T. Komatsubara, Phys. Rev. Lett. **73**, 1849 (1994).
12. T. Takahashi, N. Sato, T. Yokaya, A. Chainani, T. Morimoto, T. Komatsubara, J. Phys. Soc. Jap. **65**, 156 (1995).
13. K. Knöple, A. Mavromaras, L.M. Sandratskii, J. Kübler, J. Phys. Cond. Matter **8**, 901 (1996).
14. Y. Inada, A. Ishigura, J. Kimura, N. Sato, A. Sowada, T. Komatsubara, H. Yamagami, Physica B **206-207**, 33 (1995).
15. A. Grauel, A. Böhm, H. Fischer. C. Geibel, R. Köhler, R. Modler, C. Schank, F. Steglich, G Weber, T. Komatsubara, N. Sato, Phys. Rev. B **46**, 5818 (1992).
16. N. Sato, N. Koga, T. Komatsubara, J. Phys. Soc. Jap. **66**, 1555 (1996).
17. K. Andres, S. Darack, H.R. Ott, Phys. Rev. B **19**, 5457 (1979).
18. A. Amato, W. Bührer, A. Grayevsky, F.N. Gygax, A. Furrer, N. Kaplan, A. Schenck, Solid State Commun. **82**, 767 (1992).
19. C. Geibel, A. Böhm, R. Caspary, K. Gloos, A. Grauel, P. Hellmann, R. Modler, C. Schank, G. Weber, F. Steglich, Physica B **186-188**, 188 (1993).
20. L. Paolasini, J.A. Paixão, G.H. Lander, A. Delapalme, N. Sato, T. Komatsubara, J. Phys. Cond. Matter **5**, 8905 (1993).
21. A. Yaouanc, P. Dalmas de Réotier, G. van Laan, A. Hiess, J. Gaulon, C. Neumann, P. Lejay, N. Sato, Phys. Rev. B **58**, 8793 (1998).
22. A. Krimmel, A. Loidl, R. Eccleston, C. Geibel, F. Steglich, J. Phys. Cond. Matter **8**, 1677 (1996).
23. J. Sticht, J. Kübler, Z. Phys. B **87**, 299 (1992).
24. S. Süllow, B. Becker, A. de Visser, M. Mihalik, G.J. Nieuwenhuys, A.A. Menovsky, J.A. Mydosh, J. Phys. Cond. Matter **9**, 913 (1997).
25. see *e.g.* A. Schenck, F.N. Gygax, in *Handbook of Magnetic Materials*, edited by K.H.J. Buschow (Elsevier Science B.V., 1995), Vol. 9, Sect. 2.
26. R. Feyerherm, A. Amato, A. Grayevsky, F.N. Gygax, N. Kaplan, A. Schenck, Z. Phys. B **99**, B (1995).
27. T. Tashma, A. Amato, A. Grayevsky, F.N. Gygax, M. Pinkpank, A. Schenck, N. Kaplan, Phys. Rev. **56**, 9397 (1997).
28. A. Schenck, *Muon Spin Rotation spectroscopy - Principles and Applications in Solid State Physics* (Adam Hilger, 1985).
29. PSI - data, unpublished. The crystal was provided by B.D. Gaulin (Mc Masters University).
30. O. Hartmann, Phys. Rev. Lett. **39**, 832 (1977).
31. J.H. van Vleck, Phys. Rev. **74**, 1168 (1948).
32. R. Feyerherm, thesis ETH No. 11249 (1995); see also [11].
33. W.F. Lankford, H.K. Birnbaum, A.T. Fiory, R.P. Minnich, K.G. Lynn, C.E. Stronach, L.H. Bieman, W.J. Kossler, J. Lindemuth, Hyp. Int. **4**, 833 (1978).
34. T.P. Das, R. Bersohn, Phys. Rev. **102**, 733 (1956).
35. P.G. Akishin, I.A. Gaganov, J. Magn. Magn. Mater. **110**, 175 (1992).
36. M.J. Lysak, D.E. Mac Laughlin, Phys. Rev. B **31**, 6963 (1985) and reference therein.
37. M. Richter, M. Divis, J. Forstreuter, K. Koepernik, L. Steinbeck, H. Eschrig, Physica B (in press).
38. N.K. Sato, K. Chatani, T. Komatsubara, T. Sakon, Y. Nakanishi, M. Motokawa, preprint (1998).
39. W.W. Kim, G.R. Stewart, Phys. Rev. B **50**, 9948 (1994).